

 Open access • Journal Article • DOI:10.1086/444475

Total Galaxy Magnitudes and Effective Radii from Petrosian Magnitudes and Radii

— [Source link](#) 

Alister W. Graham, Simon P. Driver, Vahé Petrosian, Christopher J. Conselice ...+3 more authors





Institutions: Australian National University, Stanford University, California Institute of Technology, University of Wisconsin-Madison ...+1 more institutions

Published on: 01 Oct 2005 - The Astronomical Journal (University of Chicago Press)

Topics: Galaxy

Related papers:

- [The Sloan Digital Sky Survey: Technical summary](#)
- [SExtractor: Software for source extraction](#)
- [Surface Brightness and Evolution of Galaxies](#)
- [Maps of Dust Infrared Emission for Use in Estimation of Reddening and Cosmic Microwave Background Radiation Foregrounds](#)
- [Maps of Dust IR Emission for Use in Estimation of Reddening and CMBR Foregrounds](#)

Share this paper:    

View more about this paper here: <https://typeset.io/papers/total-galaxy-magnitudes-and-effective-radii-from-petrosian-4nqprgf1vn>

TOTAL GALAXY MAGNITUDES AND EFFECTIVE RADII FROM PETROSIAN MAGNITUDES AND RADII

ALISTER W. GRAHAM AND SIMON P. DRIVER

Mount Stromlo and Siding Spring Observatories, Australian National University, Private Bag, Weston Creek, ACT 2611, Australia;
graham@mso.anu.edu.au

VAHÉ PETROSIAN

Center for Space Science and Astrophysics, Department of Physics, Stanford University, Stanford, CA 94305

CHRISTOPHER J. CONSELICE¹

California Institute of Technology, Mail Code 105-24, Pasadena, CA 91125

MATTHEW A. BERSHADY AND STEVEN M. CRAWFORD

Department of Astronomy, University of Wisconsin, 475 North Charter Street, Madison, WI 53706

AND

TOMOTSUGU GOTO

Institute of Space and Astronautical Science, Japan Aerospace Exploration Agency,
3-1-1 Yoshinodai, Sagami-hara, Kanagawa 229-8510, Japan

Received 2005 April 7; accepted 2005 June 27

ABSTRACT

Petrosian magnitudes were designed to help with the difficult task of determining a galaxy’s total light. Although these magnitudes [taken here as the flux within $2R_p$, with the inverted Petrosian index $1/\eta(R_p) = 0.2$] can represent most of an object’s flux, they do of course miss the light outside the Petrosian aperture ($2R_p$). The size of this flux deficit varies monotonically with the shape of a galaxy’s light profile, i.e., its concentration. In the case of a de Vaucouleurs $R^{1/4}$ profile, the deficit is 0.20 mag; for an $R^{1/8}$ profile this figure rises to 0.50 mag. Here we provide a simple method for recovering total (Sérsic) magnitudes from Petrosian magnitudes using only the galaxy concentration (R_{90}/R_{50} or R_{80}/R_{20}) within the Petrosian aperture. The corrections hold to the extent that Sérsic’s model provides a good description of a galaxy’s luminosity profile. We show how the concentration can also be used to convert Petrosian radii into effective half-light radii, enabling a robust measure of the mean effective surface brightness. Our technique is applied to the Sloan Digital Sky Survey Data Release 2 (SDSS DR2) Petrosian parameters, yielding good agreement with the total magnitudes, effective radii, and mean effective surface brightnesses obtained from the New York University Value-Added Galaxy Catalog Sérsic $R^{1/n}$ fits by Blanton and coworkers. Although the corrective procedure described here is specifically applicable to the SDSS DR2 and DR3, it is generally applicable to all imaging data where any Petrosian index and concentration can be constructed.

Key words: galaxies: fundamental parameters — galaxies: structure — methods: analytical — methods: data analysis

1. INTRODUCTION

Galaxies are known to possess well-defined correlations between their various structural and kinematic parameters (e.g., Faber & Jackson 1976; Tully & Fisher 1977; Djorgovski & Davis 1987; Dressler et al. 1987; Caon et al. 1993; Graham et al. 2001b; De Rijcke et al. 2005; Matković & Guzmán 2005). These empirical “scaling laws” provide key observational constraints needed to test current theoretical models of galaxy formation and evolution. Obviously, even the most basic of these, the luminosity-size relation (e.g., Dutton et al. 2005; McIntosh et al. 2005), relies on our ability to accurately measure robust photometric parameters.

In this vein, the need for a more unified approach to galaxy photometry has recently been highlighted by Cross et al. (2004). They noted that much of the discrepancy in galaxy magnitudes (and sizes) between various groups is because of the varying methodology applied. For example, some authors use Kron magnitudes, others Petrosian magnitudes, some extrapolate fitted models to large radii, while others use some-

what limited aperture photometry. This can impact significantly on global measures of the galaxy population, such as the luminosity function (e.g., Norberg et al. 2002; Blanton et al. 2003a; Driver et al. 2005), the color-magnitude relation (e.g., Scodreggio 2001; Chang et al. 2005; and references therein), and the luminosity density (e.g., Yasuda et al. 2001; Cross et al. 2001). It also, for example, impacts on studies of the supermassive black hole mass function derived using the galaxy luminosity–black hole mass relation (e.g., McLure & Dunlop 2004; Shankar et al. 2004; and references therein). Perhaps less obvious, however, are the consequences for the calculation of size and surface brightness distributions (e.g., Kormendy 1977; Cross et al. 2001; Shen et al. 2003; Driver et al. 2005). These are typically derived from the half-light radius, which in turn depends critically on an accurate assessment of the total flux. If the magnitude is underestimated, the size and surface brightness distributions will be affected.

One of the great strengths of the Petrosian (1976) index, the average intensity within some projected radius divided by the intensity at that radius, and similarly the radii themselves corresponding to some fixed Petrosian index, is that they do not depend on a galaxy’s distance. That is, because surface

¹ NSF Astronomy and Astrophysics Postdoctoral Fellow.

brightness dimming does not change the shape of a galaxy's light profile it does not affect the Petrosian index, nor does it affect the observed galaxy concentration. Furthermore, due to the Petrosian index's ability to define aperture sizes that contain the bulk of an object's light, and due to the large influx of small, faint images of high-redshift galaxies that are now available, the Petrosian index has experienced a resurgence (e.g., Wirth et al. 1994; Bershady et al. 1998, 2000; Dalcanton 1998; Takamiya 1999; Volonteri et al. 2000; Blanton et al. 2001; Lubin & Sandage 2001; Conselice et al. 2002; Yagi et al. 2002). Strauss et al. (2002, their § 3.2) do, however, stress the fact that a different fraction of galaxy light is missed depending on whether a galaxy has an $R^{1/4}$ light profile or an exponential light profile, and they emphasize the subsequent need to account for this in analyses of the Sloan Digital Sky Survey (SDSS; York et al. 2000) galaxy data.

In an effort to account for the flux missed by Petrosian apertures, this paper outlines a corrective procedure to convert Petrosian magnitudes into total (Sérsic) galaxy magnitudes, as provided by popular codes such as GIM2D (Simard et al. 2002), GALFIT (Peng et al. 2002), and BUDDA (de Souza et al. 2004). The key to doing this lies in the “shape” of a galaxy's stellar distribution, that is, its concentration. This quantity may be obtained with or without the use of a fitted light profile model.

In the absence of measurement errors, all $R^{1/4}$ light profiles have exactly the same concentration index, R_{90}/R_{50} , the ratio of radii containing 90% and 50% of the Petrosian flux (e.g., Blanton et al. 2001; Strauss et al. 2002; Goto et al. 2003). The same is true for an exponential $R^{1/1}$ light profile, although the specific value of the concentration will be different in this case. It follows that the observed range of galaxy concentrations, if not due to errors, reflects a range of light profile shapes; that is, galaxies do not simply have exponential or $R^{1/4}$ light profiles.

Recognizing this in the SDSS data, Blanton et al. (2003b) adopted Sérsic's (1963, 1968) $R^{1/n}$ model² to represent the range of galaxy light profile shapes and provide estimates of their total luminosities, sizes, and surface brightnesses. Indeed, in the case of (dwarf and ordinary) elliptical galaxies, such an approach is crucial if one is to properly understand the various relationships between such terms (e.g., Graham & Guzmán 2003, their § 4). However, for low signal-to-noise ratio data or where the spatial resolution is lacking, it can become difficult to obtain reliable Sérsic fits. One therefore needs an alternative strategy to obtain the total galaxy flux and associated half-light terms.

Using only the observed concentration, R_{90}/R_{50} , within the Petrosian aperture, we provide an easy prescription to recover the total (Sérsic) flux from the Petrosian flux while maintaining the distance-independent qualities of the Petrosian system. We also explain how one can recover the effective radii and associated surface brightness terms. The corrective formulae presented here are not only valid for pure $R^{1/4}$ or exponential profiles but applicable to galaxies having intermediary light profile shapes and a range of more extreme stellar distributions.

2. PETROSIAN RADII AND MAGNITUDES

The Petrosian (1976) index was initially introduced with the goal of measuring galaxy evolution. It gained additional popularity from its potential to determine the cosmological parameters (e.g., Djorgovski & Spinrad 1981; Sandage & Perelmuter 1990). Indeed, under the assumption of structural homology it provided a means to obtain “standard rods” that could be used to constrain cosmogonic models. Nowadays, it is often used as a

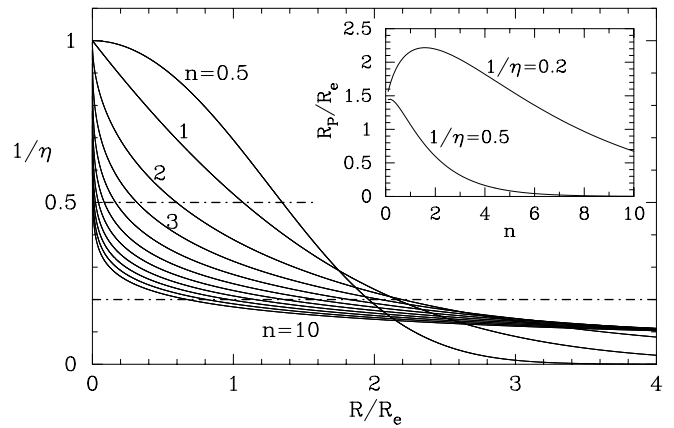


FIG. 1.—Inverted Petrosian index, $1/\eta$ (eq. [3]), as a function of normalized radius, R/R_e , for light profiles having a range of Sérsic shapes $n = 0.5, 1, 2, 3, \dots, 10$ (eq. [2]). *Inset:* Number of effective radii that the Petrosian radius R_p (the radius R at which the inverted Petrosian index equals some value) corresponds to when $1/\eta = 0.2$ and 0.5 (dot-dashed lines in the main figure).

tool for defining aperture sizes from which to measure galaxy magnitudes.

The Petrosian index, $\eta(R)$, is a function of a galaxy's projected radius, R , and can be written as

$$\eta(R) = \frac{2 \int_0^R I(R') R' dR'}{R^2 I(R)} = \frac{L(<R)}{\pi R^2 I(R)} = \frac{\langle I \rangle_R}{I(R)}, \quad (1)$$

where $I(R)$ is an object's (projected) intensity at some radius R and $\langle I \rangle_R$ is the average intensity within that radius. Following, for example, Blanton et al. (2003b), who modeled 183,487 SDSS galaxies, we adopt Sérsic's (1963) $R^{1/n}$ model to represent the possible range of light profiles $I(R)$. This can be written as

$$I(R) = I_e \exp \left\{ -b_n \left[\left(\frac{R}{R_e} \right)^{1/n} - 1 \right] \right\}, \quad (2)$$

where I_e is the intensity of the light profile at the effective radius R_e and n defines the “shape” of the profile. The term b_n is simply a function of n and chosen³ to ensure that the radius R_e encloses half the profile's total luminosity.

Using the substitution $x = b_n (R/R_e)^{1/n}$, and thus $R = x^n R_e / (b_n)^n$ and $dR = [R_e n / (b_n)^n] x^{n-1} dx$, the Petrosian index reduces to

$$\eta(x, n) = \frac{2n\gamma(2n, x)}{e^{-x} x^{2n}}, \quad (3)$$

where $\gamma(2n, x)$ is the incomplete gamma function, defined as

$$\gamma(2n, x) = \int_0^x e^{-t} t^{2n-1} dt.$$

The inverted Petrosian index, $1/\eta(R)$, is more commonly used in the literature (e.g., Bershady et al. 2000; Blanton et al. 2001) and is shown in Figure 1. It has a value of 1 at $R = 0$ and falls to zero at large radii. Although the Petrosian index can be used to determine a galaxy's “Petrosian radius” R_p (the radius at which

² A useful compilation of various Sérsic expressions can be found in Graham & Driver (2005).

³ The value b_n is such that $\Gamma(2n) = 2\gamma(2n, b_n)$, with γ and Γ the incomplete and complete gamma functions, respectively (Ciotti 1991).

the index equals some fixed value), it is important to determine the relation between this radius and the effective radius R_e ; as shown inset to Figure 1, R_p/R_e varies with Sérsic index n for a fixed $1/\eta$. Constant multiples of R_p have been used as a means to define an appropriate aperture size for purposes of deriving galaxy magnitudes. For example, some authors have chosen to use $2R_p$ with $1/\eta(R_p) = 0.2$ (e.g., Bershady et al. 2000; Blanton et al. 2001) and others $3R_p$ with $1/\eta(R_p) = 0.5$ (e.g., Conselice et al. 2002, 2003). The SDSS consortium adopted the former criteria. From Figure 1, one can see that different light profile shapes reach constant values of $1/\eta$ at different fractions of their effective half-light radii R_e . (The absolute values of R_e and I_e are not important, only the ratio R/R_e and the value of n determine $1/\eta$; see eq. [3].)

This is shown more clearly in the inset figure, where one can see, as a function of profile shape n , the number of effective radii to which $1/\eta = 0.2$ and 0.5 correspond. If $n = 4$, then $1/\eta(R_p) = 0.2$ occurs at $R_p = 1.82R_e$. However, when using $1/\eta(R_p) = 0.5$, if $n = 4$ then R_p equals only $0.16R_e$.⁴ Although this particular radius is multiplied by a factor of 3 before determining the Petrosian magnitude, this still amounts to an aperture of less than $0.5R_e$. This particular Petrosian magnitude therefore greatly underestimates an object's total magnitude.

For a Sérsic profile, the Petrosian magnitude, m_p , is given by the expression

$$m(<NR_p) = \mu_e - 5 \log R_e - 2.5 \log \left[2\pi n \frac{e^{b_n}}{(b_n)^{2n}} \gamma(2n, x_p) \right], \quad (4)$$

where $x_p = b_n(NR_p/R_e)^{1/n}$, N is the multiplicative factor (usually 2 or 3), and $\mu_e = -2.5 \log I_e$. The total magnitude is obtained by replacing $\gamma(2n, x_p)$ with the (complete) gamma function $\Gamma(2n)$.

The extent to which the Petrosian magnitude underestimates the total magnitude is shown in Figure 2 under two conditions. The first is when the Sérsic profiles extend to infinity (Fig. 2a). Although galaxies are recognized not to have sharp edges, the second condition assumes that the Sérsic profiles truncate at $5R_e$ (Fig. 2b). There is no physical justification for a truncation at $5R_e$; this is simply chosen in order to explore the magnitude deficit if the light profiles do not extend to infinity.

While elliptical galaxy light profiles continue into the background sky noise (e.g., Caon et al. 1993), there is evidence that some disk galaxies may truncate at ~ 4 scale lengths or change their exponential slope at these radii (van der Kruit 2001; Pohlen et al. 2004; Erwin et al. 2005), but see Narayan & Jog (2003) and also Bland-Hawthorn et al. (2005), who present a light profile for the late-type disk galaxy NGC 300, which extends to 10 scale lengths.

Figure 2 thus provides a boundary of sorts to the extent that Petrosian magnitudes may underestimate a galaxy's total magnitude as a function of the underlying profile shape. To avoid possible confusion, we note that R_e shall always refer to the value associated with the $R^{1/\eta}$ model extended to infinity. Thus, when the profile is assumed to truncate at $5R_e$, the value of R_e does not change.

One can see from Figure 2a that the use of $1/\eta(R_p) = 0.5$ results in magnitude differences of 0.5 mag when $n \sim 2.5$, 1.25 mag

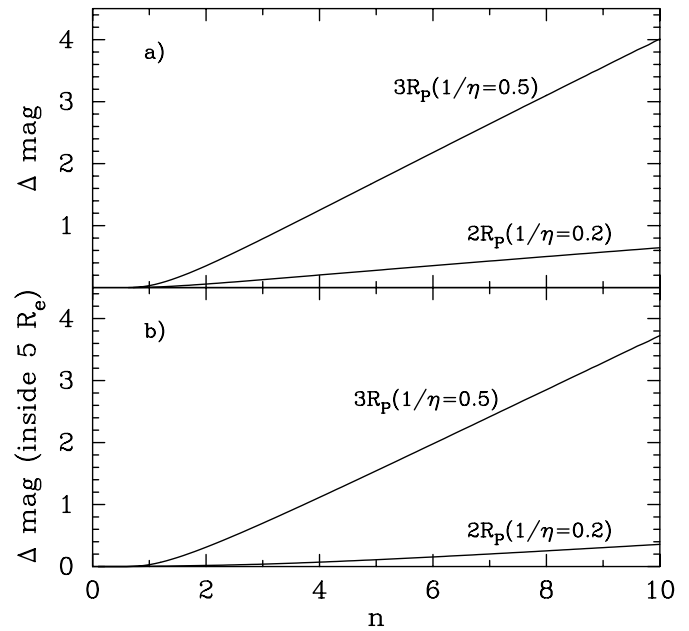


FIG. 2.—(a) Difference, as a function of light profile shape n , between the Petrosian magnitude (eq. [4]) inside twice the radius where $1/\eta = 0.2$ and thrice the radius where $1/\eta = 0.5$ and the total magnitude obtained by integrating the $R^{1/\eta}$ profile to infinity. (b) Similar to (a) but assuming that the $R^{1/\eta}$ light profiles are truncated at $5R_e$.

when $n = 4$, 2 mag when $n \sim 5.5$, and considerably worse for galaxies with yet higher values of n . Obviously, such an approach to determine galaxy magnitudes should be used with caution. When dealing with dwarf galaxies, because of their faint central surface brightnesses the sky flux can often dominate at the radius where $1/\eta(R_p) = 0.2$. The use of $1/\eta(R_p) = 0.5$ is thus more practical, and for galaxies with $n \lesssim 2$ the bulk of their flux is still recovered.

Overall, however, the use of $1/\eta(R_p) = 0.2$ does much better at recovering a galaxy's true magnitude.⁵ When $n = 4$, the magnitude difference⁶ is only 0.20 mag, rising to 0.64 mag when $n = 10$.

Things are better for profiles with smaller values of n and if one considers that the profiles truncate at $5R_e$ (Fig. 2b).

3. RECOVERING EFFECTIVE RADII AND TOTAL (SÉRSIC) MAGNITUDES

In this section we only consider the case in which $1/\eta(R_p) = 0.2$, using $2R_p$ to define the Petrosian magnitude. The merits of this precise definition, which was used by the SDSS team, are exalted in Strauss et al. (2002, their § 3.2).

3.1. Concentration

If one had some way of knowing the underlying light profile shape n , then from Figure 2 one could correct the Petrosian magnitudes for the missing flux beyond $2R_p$. Given that the Petrosian index was developed in part to avoid fitting a model to

⁴ Although § 3.3 of Bershady et al. (2000) reports that $1/\eta(R_p) = 0.5$ roughly corresponds to $R_p = 1R_e$, this is only true for Sérsic profiles with $n \lesssim 2$ (see Fig. 1). Exact values for R_p , in terms of R_e , when $1/\eta(R_p) = 0.5$ are given in Bershady et al. (1998) for $n = 0.5, 1$, and 4.

⁵ The use of $1/\eta(R_p) = 0.2$ has also been adopted by some authors because it results in a minimal variation of R_p/R_e with n . For $n \lesssim 4$, this value is around 2, and so to approximate the total light one could measure the light within $R_p/2$ and multiply by 2.

⁶ Bershady et al. (2000) reported a difference of 0.13 mag, but this is appropriate for an $n = 3$ profile rather than an $n = 4$ profile. The value of 0.13 mag was based on photometry of IRAF ARTDATA simulations and therefore is likely to be a round-off or discretization error in the IRAF rendering.

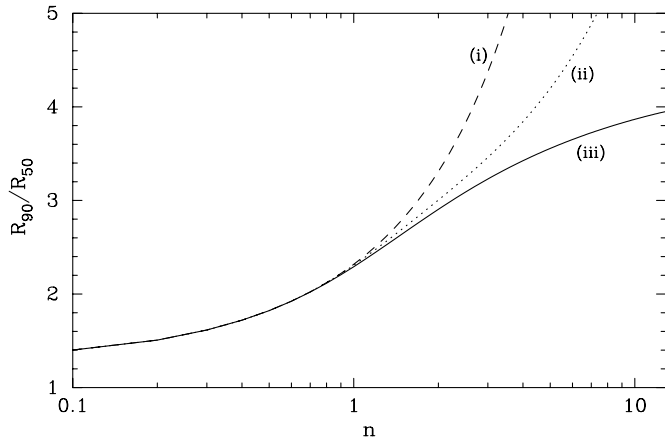


FIG. 3.—Concentration index, defined as the ratio of radii R_{90}/R_{50} , as a function of the light profile shape n . (i) R_{90} and R_{50} are simply the radii containing 90% and 50% of the total flux (obtained by integrating the Sérsic profile to infinity; note that $R_{50} = R_e$ in this case). (ii) Similar to (i) except that the total flux is now considered to be only that within $5R_e$ (i.e., the Sérsic profile is truncated at $5R_e$). (iii) R_{90} and R_{50} are now the radii containing 90% and 50% of the flux within NR_p , where we have chosen $N = 2$ and R_p is the Petrosian radius such that $1/\eta(R_p) = 0.2$.

an object’s light profile, one may prefer not to fit the $R^{1/n}$ model, or indeed one may not have the resolution to do so.

Conveniently, central light “concentration” is monotonically related to the shape of a light profile (Trujillo et al. 2001c; Graham et al. 2001a). One can therefore use concentration as a proxy for the value of n .

The SDSS consortium have been using a ratio of two radii (R_{90} and R_{50}) as a measure of an object’s concentration, both of which are available from the SDSS public data releases. These radii enclose 90% and 50% of the Petrosian flux, and their ratio is shown in Figure 3 and Table 1 as a function of the underlying light profile shape n .

The use of such radii avoids the inner seeing-affected part of a light profile and also avoids the outer noisier part of a profile while still providing a useful range of concentrations for the various galaxies. For an $n = 1$ and an $n = 4$ profile,⁷ R_{90}/R_{50} equals 2.29 and 3.42, respectively. The inverse ratio is sometimes used, giving 0.44 and 0.29 (Blanton et al. 2001, their § 4.5). Not surprisingly, the R_{90}/R_{50} concentration index correlates with galaxy type and also color (e.g., Strateva et al. 2001; Kauffmann et al. 2003).

3.2. Magnitudes

Combining Figures 2 and 3, Figure 4a shows the required magnitude correction in order to account for the missing flux beyond the Petrosian aperture $2R_p$, when $1/\eta(R_p) = 0.2$, as a function of concentration within the Petrosian aperture (i.e., curve [iii] from Fig. 3). When $n = 4$, $R_{90}/R_{50} = 3.42$ and $\Delta\text{mag} = 0.20$ and 0.07 mag to recover the total flux and that within $5R_e$, respectively (see Table 1).

To an accuracy of ~ 0.01 mag, over the Sérsic interval $0.1 < n < 10$ the missing flux (Fig. 4a) can be approximated by the expression

$$\Delta m \approx P_1 \exp\left[(R_{90}/R_{50})^{P_2}\right] \equiv m_p - m_x, \quad (5)$$

⁷ If an $n = 1$ and an $n = 4$ profile are integrated to infinity rather than only $2R_p$, then $R_{90} = 2.32R_e$ and $5.55R_e$, respectively.

where P_1 and P_2 equal 5.1×10^{-4} and 1.451 in order to recover the total flux (Fig. 5a), and 5.9×10^{-5} and 1.597 in order to recover the flux within $5R_e$ (Fig. 5b). Here m_p is the Petrosian magnitude and m_x is the corrected magnitude, which, to an accuracy of ~ 0.01 mag, is equivalent to the Sérsic magnitude (m_s).

3.3. Radii

The effective radii containing half of the total (Sérsic) flux can be computed in a number of ways.

Figure 4b is the combination of Figure 3 and the inset figure from Figure 1, and allows one to determine the effective radius R_e from the Petrosian radius and concentration R_{90}/R_{50} within the Petrosian aperture. Alternatively, from the total galaxy magnitude (approximated by m_x) one may empirically determine the aperture containing half a galaxy’s light and therefore obtain the half-light radius this way.

As a further alternative, for $0.1 < n < 10$ the R_{50}/R_e curve seen in Figure 4c can be approximated in terms of Petrosian concentration by the expression

$$R_e \approx \frac{R_{50}}{1 - P_3 (R_{90}/R_{50})^{P_4}} \equiv R_x, \quad (6)$$

where P_3 and P_4 equal 8.0×10^{-6} and 8.47, respectively. This approximation is shown in Figure 5c.

3.4. Surface Brightnesses

It turns out that one can also easily transform μ_{50} , the surface brightness at R_{50} , and $\langle \mu \rangle_{50}$, the mean surface brightness within R_{50} , into the effective surface brightness, μ_e , and the mean effective surface brightness $\langle \mu \rangle_e$. From Graham & Driver (2005, their eq. [6] and their § 2.2), one has that

$$\mu_{50} - \mu_e = \frac{2.5b_n}{\ln 10} \left[\left(\frac{R_{50}}{R_e} \right)^{1/n} - 1 \right], \quad (7)$$

and

$$\langle \mu \rangle_{50} - \langle \mu \rangle_e = 2.5 \log \left[\left(\frac{R_{50}}{R_e} \right)^2 \frac{\gamma(2n, x_e)}{\gamma(2n, x_{50})} \right], \quad (8)$$

where $x_{50} = b_n(R_{50}/R_e)^{1/n}$ and $x_e = b_n$.

One can see that for a given value of n , the ratio R_{50}/R_e (Fig. 4c) is sufficient to solve equations (7) and (8). Again using the relation between n and R_{90}/R_{50} (Fig. 3, curve [iii]), Figures 4d and 4e show the surface brightness differences as a function of the concentration R_{90}/R_{50} .

In practice, one can directly measure the surface brightness at R_e and/or the mean surface brightness within R_e , the latter of which can also be computed from the expression $L_{\text{tot}} = 2\pi R_e^2 \langle I \rangle_e$. Approximations to equations (7) and (8) are therefore not given.

Because the above values of R_e , μ_e , and $\langle \mu \rangle_e$ are those pertaining to a nontruncated Sérsic profile, equations (6)–(8) are independent of any possible profile truncation beyond the Petrosian aperture.

4. APPLICATION

4.1. Demonstration with SDSS Data

The SDSS consortium adopted a slightly modified form of the Petrosian index. Rather than dividing the average intensity within R_p by the intensity at R_p (eq. [1]), they divided the

TABLE 1
PETROSIAN RADII, CONCENTRATION, AND MAGNITUDE CORRECTIONS

n (1)	R_p (R_e) (2)	R_{50} (R_e) (3)	R_{90}/R_{50} (4)	R_{50}/R_{90} (5)	$\mu_e - \mu_{50}$ (mag arcsec $^{-2}$) (6)	$\langle \mu \rangle_e - \langle \mu \rangle_{50}$ (mag arcsec $^{-2}$) (7)	ΔM_∞ (mag) (8)	ΔM_{5R_e} (mag) (9)
Standard Petrosian: Aperture equals $2R_p(1/\eta = 0.2)$, η given in eq. (3)								
0.1.....	1.57	1.00	1.40	0.71	0.00	0.00	0.00	0.00
0.2.....	1.70	1.00	1.51	0.66	0.00	0.00	0.00	0.00
0.3.....	1.80	1.00	1.62	0.62	0.00	0.00	0.00	0.00
0.5.....	1.96	1.00	1.82	0.55	0.00	0.00	0.00	0.00
0.7.....	2.06	1.00	2.02	0.49	0.00	0.00	0.00	0.00
1.0.....	2.16	0.99	2.29	0.44	0.01	0.01	0.01	0.00
2.0.....	2.20	0.93	2.90	0.34	0.13	0.09	0.06	0.02
3.0.....	2.04	0.84	3.23	0.31	0.36	0.26	0.13	0.04
4.0.....	1.82	0.73	3.42	0.29	0.63	0.48	0.20	0.07
5.0.....	1.59	0.62	3.56	0.28	0.94	0.74	0.28	0.11
6.0.....	1.36	0.53	3.65	0.27	1.27	1.03	0.35	0.15
7.0.....	1.15	0.44	3.72	0.27	1.62	1.33	0.43	0.20
8.0.....	0.97	0.37	3.78	0.26	1.98	1.65	0.50	0.25
9.0.....	0.81	0.31	3.83	0.26	2.35	1.98	0.57	0.30
10.0.....	0.67	0.25	3.87	0.26	2.73	2.33	0.64	0.36
SDSS Petrosian: Aperture equals $2R_p(1/\eta = 0.2)$, η given in eq. (9)								
0.1.....	1.63	1.00	1.40	0.71	0.00	0.00	0.00	0.00
0.2.....	1.72	1.00	1.51	0.66	0.00	0.00	0.00	0.00
0.3.....	1.81	1.00	1.62	0.62	0.00	0.00	0.00	0.00
0.5.....	1.94	1.00	1.82	0.55	0.00	0.00	0.00	0.00
0.7.....	2.03	1.00	2.02	0.49	0.00	0.00	0.00	0.00
1.0.....	2.11	0.99	2.29	0.44	0.01	0.01	0.01	0.01
2.0.....	2.12	0.93	2.88	0.35	0.15	0.10	0.06	0.02
3.0.....	1.94	0.82	3.17	0.32	0.38	0.28	0.14	0.05
4.0.....	1.71	0.71	3.35	0.30	0.68	0.52	0.22	0.09
5.0.....	1.48	0.61	3.47	0.29	1.00	0.79	0.30	0.13
6.0.....	1.25	0.51	3.55	0.28	1.35	1.09	0.38	0.18
7.0.....	1.05	0.42	3.62	0.28	1.72	1.41	0.46	0.23
8.0.....	0.88	0.35	3.67	0.27	2.09	1.74	0.54	0.29
9.0.....	0.72	0.29	3.71	0.27	2.48	2.09	0.61	0.34
10.0.....	0.60	0.24	3.74	0.27	2.87	2.45	0.69	0.40
CAS Petrosian: Aperture equals $1.5R_p(1/\eta = 0.2)$, η given in eq. (3)								
0.1.....	1.57	1.00	2.04 ^a	0.49 ^b	0.00	0.00	0.00	0.00
0.2.....	1.70	1.00	2.17	0.46	0.00	0.00	0.00	0.00
0.3.....	1.80	1.00	2.33	0.43	0.00	0.00	0.00	0.00
0.5.....	1.96	1.00	2.68	0.37	0.00	0.00	0.00	0.00
0.7.....	2.06	0.99	3.03	0.33	0.01	0.01	0.01	0.01
1.0.....	2.16	0.97	3.53	0.28	0.05	0.03	0.03	0.03
2.0.....	2.20	0.88	4.96	0.20	0.26	0.17	0.12	0.08
3.0.....	2.04	0.76	6.16	0.16	0.54	0.39	0.20	0.11
4.0.....	1.82	0.65	7.20	0.14	0.86	0.66	0.29	0.16
5.0.....	1.59	0.55	8.12	0.12	1.20	0.95	0.37	0.20
6.0.....	1.36	0.46	8.96	0.11	1.56	1.26	0.45	0.25
7.0.....	1.15	0.38	9.72	0.10	1.92	1.58	0.53	0.30
8.0.....	0.97	0.31	10.43	0.10	2.30	1.92	0.60	0.35
9.0.....	0.81	0.26	11.08	0.09	2.68	2.27	0.68	0.41
10.0.....	0.67	0.21	11.67	0.09	3.07	2.62	0.75	0.46

NOTES.—Col. (1): Sérsic index n . Col. (2): Petrosian radius R_p such that $1/\eta(R_p) = 0.2$. Col. (3): Radius containing 50% of the Petrosian flux. Col. (4): Concentration index defined by the ratio of radii that contain 90% and 50% of the Petrosian flux. Col. (5): The inverse of col. (4). Col. (6): Difference between the surface brightness at R_e and the value at R_{50} . Col. (7): Difference between the mean surface brightness inside the radii R_e and that at R_{50} . Col. (8): Difference between the Petrosian magnitude and the total magnitude (obtained by integrating the Sérsic profile to infinity). Col. (9): Difference between the Petrosian magnitude and the Sérsic magnitude if the profile is truncated at $5R_e$.

^a For the column in this section of the table, the concentration index is defined by the ratio of radii that contain 80% and 20% of the Petrosian flux.

^b This column is again the inverse of col. (4) (20% to 80% ratio).

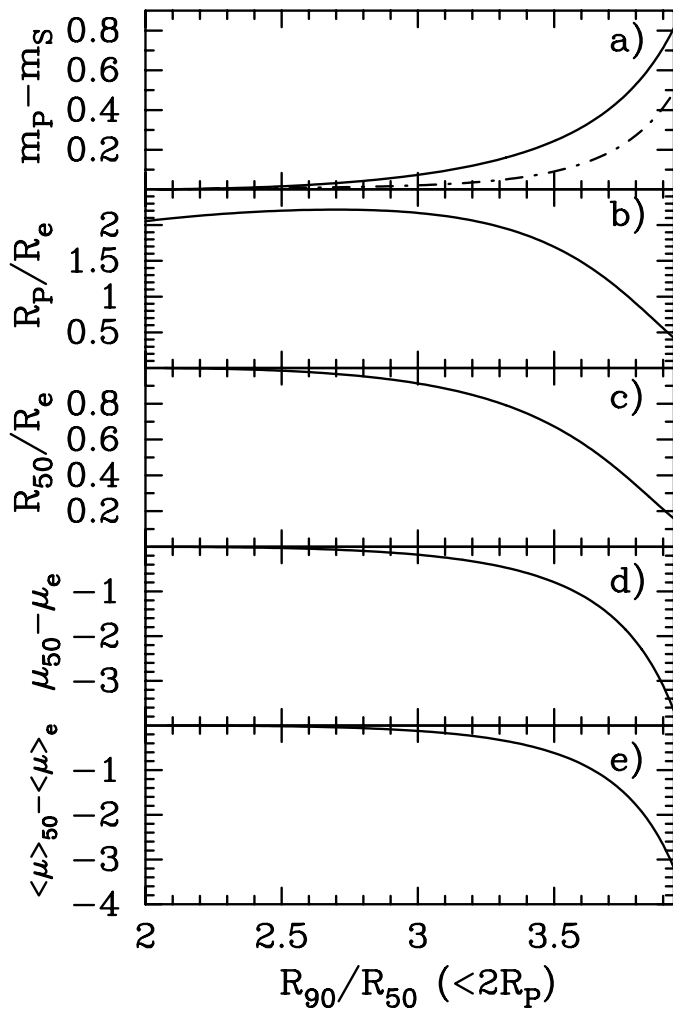


FIG. 4.—(a) Magnitude differences shown in Fig. 2 for the $1/\eta(R_p) = 0.2$ curves vs. the associated Petrosian concentration index R_{90}/R_{50} within the Petrosian aperture $2R_p$ (as shown by curve [iii] in Fig. 3). The solid curve gives the correction to obtain the total (Sérsic) magnitude, while the dash-dotted curve gives the correction if the underlying Sérsic profile is truncated at $5R_e$. (b) Ratio of Petrosian radii R_p [where $1/\eta(R_p) = 0.2$] to effective radii R_e . (c) Radius containing 50% of the Petrosian flux, R_{50} , divided by the effective radius R_e . (d) Difference between the surface brightness at R_{50} and that at R_e . (e) Difference between the mean surface brightness within R_{50} and the mean surface brightness within R_e . All panels are relative to R_{90}/R_{50} within $2R_p$ and with $1/\eta(R_p) = 0.2$ using the “standard” definition for the Petrosian index (eq. [3]).

average intensity within R_p by the average intensity within $0.8R_p$ – $1.25R_p$. This was done to reduce the sensitivity of the index to noise and (possible) real small-scale fluctuations in the light profile (Strauss et al. 2002). As a result, their definition of the Petrosian index is given by the expression

$$\eta(x, n) = \frac{\gamma(2n, x_{1.25R}) - \gamma(2n, x_{0.8R})}{[(1.25)^2 - (0.8)^2] \gamma(2n, x)}, \quad (9)$$

where $x_{1.25R} = b_n(1.25R/R_e)^{1/n}$ and $x_{0.8R} = b_n(0.8R/R_e)^{1/n}$.

In general, where the SDSS Petrosian index (eq. [9]) equals 1/0.2 the associated Petrosian radii are slightly smaller than the radii obtained previously with equation (3) equal to 1/0.2 (see Table 1). The required magnitude corrections are therefore slightly greater when using the SDSS definition.

The overall appearance of Figures 1–4 does not change, but the exact numbers are different by a few percent and therefore are provided in Table 1. The approximations given by equations (5)

and (6) also require a slight modification. Using the SDSS definition of the Petrosian index (eq. [9]), to recover the total magnitude one now has $P_1 = 4.2 \times 10^{-4}$ and $P_2 = 1.514$ (Fig. 5d), and to recover the flux within $5R_e$ one has $P_1 = 8.0 \times 10^{-5}$ and $P_2 = 1.619$ (Fig. 5e). The values for P_3 and P_4 are 6.0×10^{-6} and 8.92, respectively (see Fig. 5f).

We have tested the applicability and need for these corrections using real data from the SDSS consortium. Specifically, we have taken the Petrosian magnitudes, 50% Petrosian radii, and surface brightnesses (m_p , R_{50} , and $\langle \mu \rangle_{50}$) from the SDSS Second Data Release⁸ (Abazajian et al. 2005) and the Sérsic-derived total magnitudes, effective radii, and surface brightnesses (m_s , R_e , and $\langle \mu \rangle_e$) from the New York University Value-Added Galaxy Catalog (NYU-VAGC; Blanton et al. 2005).⁹ From this sample we then removed those galaxies whose Petrosian-derived R_{50} values are biased high by seeing; we crudely did this by excluding galaxies with $R_e < 5''$ (90% of SDSS DR2 seeing was between $1''0$ – $1''6$).

In deriving Sérsic parameters, Blanton et al. (2005) prevented the fits from obtaining Sérsic indices greater than 5.9 (and less than 0.2). To avoid any objects piled up at this boundary, and which therefore may not have accurate Sérsic quantities, we only use galaxies with $n < 5.8$ (and greater than 0.21). This left us with a sample of 16,128 galaxies, more than enough to test our method.¹⁰

Figure 6 plots the difference between the Petrosian and Sérsic values as a function of the (SDSS tabulated) concentration indices R_{90}/R_{50} within the Petrosian apertures. A similar figure using Sérsic n rather than concentration is given in Blanton et al. (2003a, their Figure 14).

The solid curves show the expected differences that we have derived. The dashed curves show the selection boundary imposed on the data due to the restriction used by Blanton et al. (2005). Confining n to values smaller than 5.8 can prevent an accurate recovery of the total Sérsic flux in large galaxies and (artificially) prevents Sérsic magnitudes getting more than 0.37 mag brighter than the SDSS-defined Petrosian magnitudes (see Table 1). Of course, measurement errors in either the Petrosian or Sérsic magnitude, and also real deviations from a Sérsic profile, can result in differences outside this selection boundary.

In Figure 6a, the Sérsic magnitudes are clearly brighter than the Petrosian magnitudes for concentrations greater than about 2.7 ($n \sim 1.7$). In Figure 6b it is obvious that our corrected Petrosian magnitudes agree with the Sérsic magnitudes, at least to a concentration of ~ 3.3 ($n \sim 4$), at which point the selection boundary from the Sérsic fits start to dominate the figure.

In the concentration bin $2.75 \leq R_{90}/R_{50} < 3.0$, the mean difference between the Petrosian and Sérsic magnitudes, $\langle m_p - m_s \rangle$, equals 0.087 ± 0.005 mag, close to the expected offset of 0.06 mag at $R_{90}/R_{50} = 2.87$ (the mean concentration inside this bin). In this same bin, $\langle m_x - m_s \rangle = 0.027 \pm 0.005$ mag. In the next bin, $3.0 \leq R_{90}/R_{50} < 3.25$ and $\langle m_p - m_s \rangle = 0.144 \pm 0.004$ mag, with the expected value at $R_{90}/R_{50} = 3.12$ (the mean concentration inside this bin) equal to 0.13 mag. Similarly, $\langle m_x - m_s \rangle = 0.028 \pm 0.004$ mag in this bin.

⁸ SDSS DR2; see <http://www.sdss.org/dr2>.

⁹ For more information on NYU-VAGC, see <http://sdss.physics.nyu.edu/vagc>.

¹⁰ For those who need or wish to use the full galaxy sample, the seeing-affected radii R_{50} will first need to be corrected (see Trujillo et al. [2001a, 2001b] for a prescription to do this). The Sérsic radii R_e were obtained by Blanton et al. (2005) from the application of seeing-convolved Sérsic profiles and therefore need no further seeing correction.

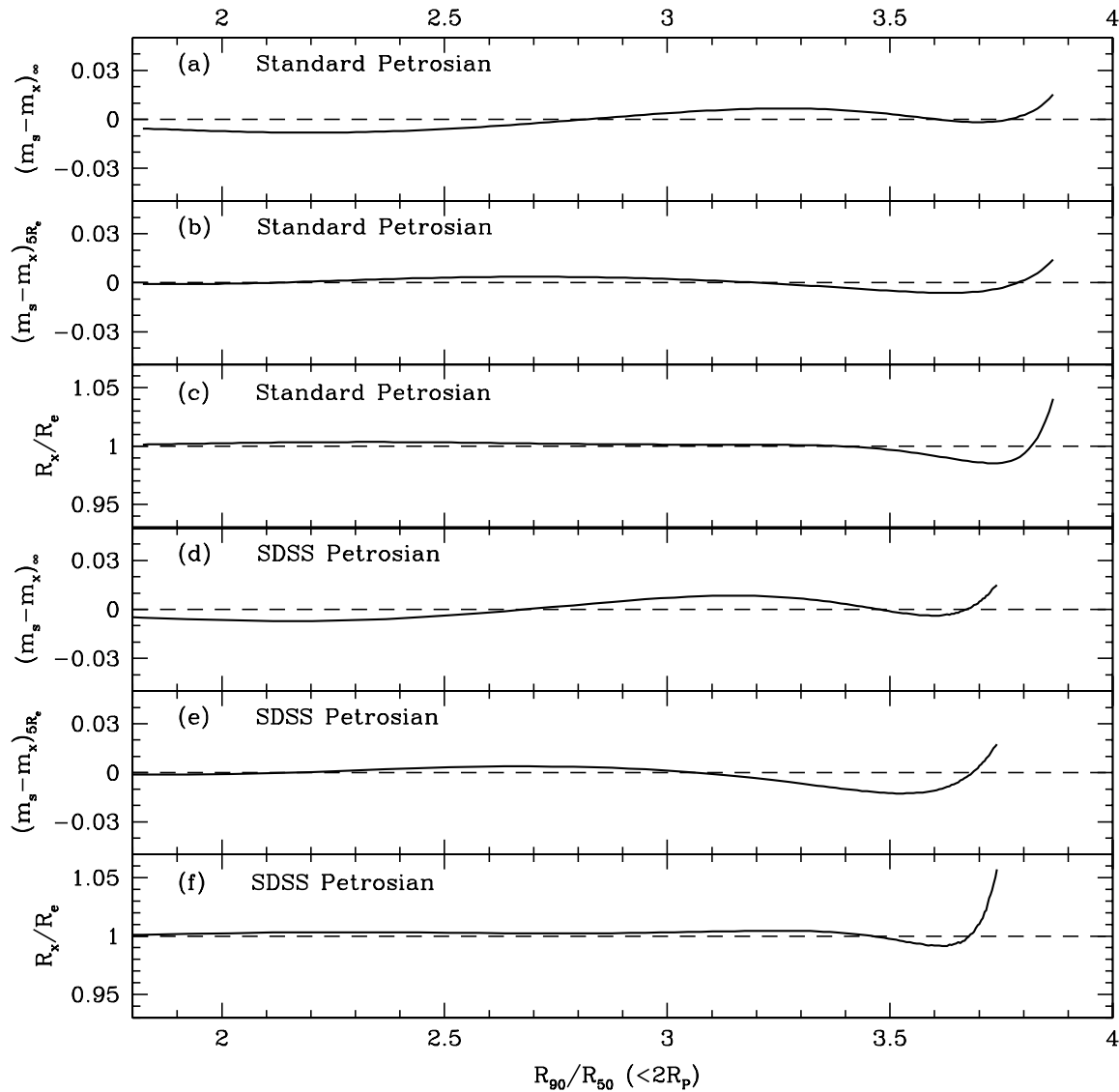


FIG. 5.—(a, b) Difference between the exact magnitude corrections seen in Fig. 4a and the approximate magnitude corrections given by eq. (5). (c) Relative error in the radius R_x , the approximation used to represent the effective radius R_e (eq. [6]). (d–f) Similar to (a–c) but based on the SDSS definition of the Petrosian index (eq. [9]).

The mean value of R_{90}/R_{50} in the bin $3.25 \leq R_{90}/R_{50} < 3.5$ is 3.34, for which the expected value of $\langle m_p - m_s \rangle$ is 0.22 mag. However, the measured value is only 0.148 ± 0.006 mag. The reason for this is partly due to the selection boundary but is primarily due to the underestimation of the Sérsic magnitude by Blanton et al. (2005). Figure 9 from Blanton et al. reveals that at $n = 4$, corresponding to $R_{90}/R_{50} = 3.35$, their Sérsic fluxes are underestimated by $\sim 7\%$. This therefore accounts for the value of 0.148 ± 0.006 mag instead of ~ 0.22 and for the negative value of $\langle m_x - m_s \rangle = -0.063 \pm 0.006$ mag in this bin.

For a system with $n = 5$, Blanton et al. (2005) typically obtained $n = 4.0$ – 4.6 and recovered only $\sim 90\%$ of the actual flux from their simulated test galaxies. The situation is systematically worse for galaxies with higher values of n and accounts for much of the apparent overcorrection in Figure 6b at high concentrations. Due to this problem, the simple corrective procedure presented here to allow for the missing flux outside the Petrosian aperture actually provides a means to acquire (total) Sérsic magnitudes that are more accurate than those obtained from the direct application of Sérsic models to the data. For a typical elliptical

galaxy, our method improves the accuracy on the galaxy magnitude from a couple of tenths of a mag to a couple of hundredths of a mag (assuming that the Sérsic profile within the Petrosian aperture continues outside of it).

We note that $>99\%$ of the SDSS Main Galaxy Sample ($m_r < 17.77$) have $R_{90}/R_{50} < 3.5$ (Blanton et al. 2003b). Thus, cases in which corrections are most severe are rare. This, however, is not to say that the high-concentration objects are uninteresting. Due to the M_{bh} -concentration relation (Graham et al. 2001a), they are the galaxies expected to have the most massive supermassive black holes.

In passing we also note that Figures 6a and 6b reveal that the SDSS Petrosian magnitudes are too faint, in the sense that they underestimate the total galaxy flux, at the high-luminosity end. Correcting for this increases the galaxy number counts at the bright end of the (Petrosian derived) luminosity function (see Blanton et al. 2003a).

Figure 6c shows the difference between the Petrosian radii R_{50} and the Sérsic effective radii. There is a clear offset at the high-concentration end of the diagram, albeit constrained

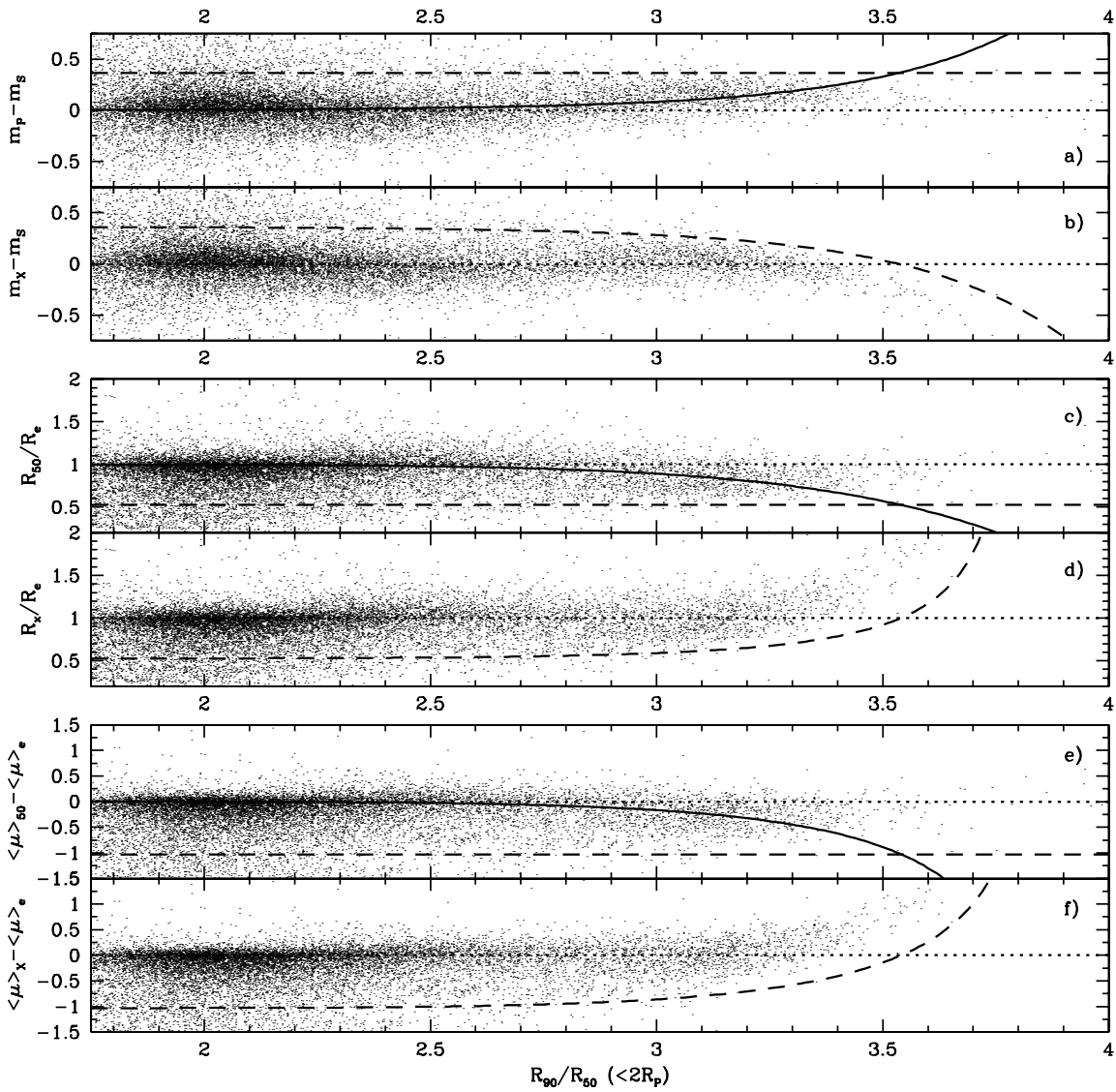


FIG. 6.—(a) Difference between the SDSS Petrosian magnitude m_P and the NYU-VAGC Sérsic magnitudes m_S as a function of concentration for 16,128 galaxies. The solid curve is the expected difference based on the correction we have formulated to obtain the flux beyond the Petrosian aperture. The dashed line reflects the selection boundary imposed on the data by the restriction that $n \lesssim 5.9$ in the Sérsic fitting process used by Blanton et al. (2003b). We made a cut at $n = 5.8$ to avoid any galaxies that may have piled up at the upper boundary to n . (b) Our corrected Petrosian magnitudes m_x vs. the Sérsic magnitudes. The selection boundary in (a) has been propagated into this panel. (c) Petrosian 50% radii R_{50} divided by the Sérsic effective radii R_e vs. concentration. From Table 1, one can see that the restriction that n be less than 5.8 (artificially) prevents R_{50}/R_e from getting smaller than 0.53. (d) Our corrected values for R_{50} , denoted here by R_x , are shown divided by the Sérsic radii R_e . Again we have propagated the selection boundary. (e, f) Similar to the other panels but showing the mean surface brightness.

within the selection boundary that prevented Sérsic indices greater than 5.8 and thus, from Table 1, $R_{50}/R_e < 0.53$. At the concentration $R_{90}/R_{50} = 3.4$, $n \sim 4.5$, and from Figure 9 in Blanton et al. (2005) one can see that their Sérsic effective radii are only $\sim 80\%$ of the true effective radii. Allowing for this, the average ratio R_x/R_e should be ~ 1.25 at $R_{90}/R_{50} = 3.4$, exactly as observed in Figure 6d. That is to say, the apparent mismatch at high concentrations is understood; it arises from the systematics that Blanton et al. (2005) identified in their fitted Sérsic quantities.

Figure 6e reveals that the early-type galaxies, defined to be those with concentrations greater than 2.86 (e.g., Shimasaku et al. 2001), have Petrosian surface brightnesses that are clearly brighter than the Sérsic-derived surface brightness. Figure 6f shows that the procedure does a good job at correcting for the missing flux beyond the Petrosian apertures, at least until a concentration of around 3.3, at which point the selection boundary

and the underestimation of the Sérsic flux once more come into play.

4.2. Application in CAS Space

Another popular setup is that used in the CAS system (Conselice 2003), which measures the concentration (C), asymmetry (A), and stellar/star-forming clumpiness (S) of a galaxy's light distribution. Within the CAS code, Petrosian apertures have sizes of $1.5R_p$, with $1/\eta(R_p) = 0.2$. Concentration is also defined slightly differently from that used by the SDSS consortium; it is the ratio of radii containing 80% and 20% (rather than 90% and 50%) of the flux within the Petrosian aperture (Bershady et al. 2000).

Theoretically, it does not matter what choice of radii one uses to define concentration. For example, radii containing 100% and 50% of the flux within the Petrosian aperture would work. In practice, the use of a large upper percentage and a

small lower percentage leads to a greater range of concentrations and thus a clearer distinction between different profile types. However, not using too large an upper percentage allows one to work with a less noisy part of the light profile. Not using too small a lower percentage means that one is less vulnerable to the effects of seeing. An analysis of the optimal concentration index (e.g., Graham et al. 2001a) is, however, beyond the intended scope of this paper and will be addressed elsewhere. We note that such a search need not be limited to differing percentages but could include radii based on different values of the Petrosian index. Here we simply provide the corrections using the popular SDSS and CAS definitions for the concentration index and Petrosian index/aperture.

The various size and flux transformation and corrective terms for the specific Petrosian setup [$1.5R_p$, with $1/\eta(R_p) = 0.2$] and concentration (R_{80}/R_{20}) used by the CAS code of Conselice et al. (2003) are given in Table 1. To approximate the total Sérsic magnitude over a range in n from 0.1 to 10, this missing flux Δm can be approximated by

$$\begin{aligned} \Delta m &\approx -0.096 + 0.021(R_{80}/R_{20}) + 0.0044(R_{80}/R_{20})^2 \\ &\equiv m_p - m_x. \end{aligned} \quad (10)$$

To obtain the flux within $5R_e$, the following provides a good approximation:

$$\Delta m \approx -0.012 - 0.0013(R_{80}/R_{20}) + 0.00346(R_{80}/R_{20})^2. \quad (11)$$

The effective Sérsic radius R_e is given by

$$\begin{aligned} R_{50}/R_e &\approx 0.903 + 0.102(R_{80}/R_{20}) - 0.0276(R_{80}/R_{20})^2 \\ &\quad + 0.00119(R_{80}/R_{20})^3. \end{aligned} \quad (12)$$

4.3. General Applicability

Caon et al. (1993) have shown that Sérsic's $R^{1/n}$ model fits early-type galaxies remarkably well (see their Fig. 2) down to faint surface brightness levels ($\mu_B \sim 27$ mag arcsec $^{-2}$). Spiral galaxies, however, usually have two clearly distinct components, namely, a bulge and a disk. It is therefore pertinent to inquire how the above corrections may apply when a galaxy is clearly better represented by two components, as is the case for the intermediate-type galaxies.

When dealing with luminous galaxies, the rough divide between early- and late-type galaxies has been taken to occur at $R_{90}/R_{50} = 2.86$ ($n \sim 2$) (Shimasaku et al. 2001; Shen et al. 2003, using the SDSS definition of Petrosian index and aperture).¹¹ It should be kept in mind that this concentration-based definition of galaxy type is only applicable to luminous systems. Dwarf elliptical galaxies have exponential-like profiles and thus low concentrations (e.g., Graham et al. 2001a, their Fig. 8) but are obviously not late-type galaxies.

The magnitude correction for galaxies having concentrations of this size or smaller is less than 0.06 mag (Table 1). In late-type galaxies, the exponential disk, rather than the bulge, dominates the flux in the outer parts. Whether or not these disks continue for many scale lengths or truncate at a few scale lengths, if one applies the corrections presented here one will not overcorrect the galaxy flux by more than 0.06 mag for the two-component

late-type galaxies, nor overestimate the half-light radius by more than 7% (Table 1).

If, however, one is able to identify the disk-dominated galaxies from their blue rest-frame colors, or indeed from their low concentrations (assuming that no low-luminosity elliptical galaxies reside in one's sample, or folding in asymmetry to separate the galaxy classes), then one may instead elect to apply the small corrections applicable for systems with an $n = 1$ (exponential disk) light profile. Given that the corrections for such stellar distributions are small, a simple answer may then be to only apply the various corrections to the red galaxy population or to systems with (SDSS) concentrations greater than, e.g., 2.86.

We caution that intermediate objects, such as lenticular galaxies, with half their light coming from their disk and half from their bulge, may not be well approximated with a single Sérsic profile. In such cases the concentration prescription given here should be used with care, as it is intended for systems that can be approximated with a single Sérsic function. In general, however, § 4.1 and in particular Figure 6 reveal that the method developed here seems to work rather well.

A different issue pertains to how one actually measures the Petrosian index. For a disk system, the Petrosian index is independent of disk inclination if one uses appropriate elliptical apertures reflecting the inclination of the disk. If one instead measures the index from the slope of the major axis light profile, such that $2/\eta = d[\ln L(R)]/d(\ln R)$ (Gunn & Oke 1975), then again the index is not dependent on the inclination of the disk. However, the use of circular apertures applied to highly inclined disk galaxies will result in erroneously high concentrations compared to what these values would be if such galaxies were viewed with a face-on orientation. Although we have not quantified this effect, comparisons between eyeball morphology and concentration index yields reasonable agreement for the late-type galaxies (e.g., Shimasaku et al. 2001), suggesting that in practice this effect is not a significant problem.

Lastly, we note that if image distortion due to seeing is not corrected for and is such that the point-spread function has altered the Petrosian 50% radius R_{50} and thus R_{90}/R_{50} (or R_{80}/R_{20}) to the extent that the measured value no longer reflects the intrinsic galaxy concentration, then obviously one should not be including such objects in plots or analyses that use this quantity. The concentration-based corrections outlined in this study cannot be applied in such circumstances, at least until the radii are corrected for seeing (e.g., Trujillo et al. 2001a, 2001b). We also direct readers to Blanton et al. (2001), who present a study of how the SDSS Petrosian magnitudes are affected by seeing, and Wirth et al. (1994), who considered the affects of both poor image resolution and low signal-to-noise ratio on image concentration.

5. SUMMARY

In commenting on the adopted Petrosian system of the SDSS consortium, Strauss et al. (2002) wrote that ‘‘Any scientific analysis that uses the [SDSS] redshift survey must consider how the fact that a different fraction of light is included for elliptical and spiral galaxies affects the result.’’ This was both a recognition that (1) their particular Petrosian system likely captures a different fraction of galaxy light compared to other surveys and that (2) any practical definition of Petrosian parameters will inevitably miss some fraction of a galaxy's light and a different fraction in different galaxies. For example, a galaxy with an exponential light profile will have 99% of its total flux encompassed by the SDSS Petrosian magnitude, but if a galaxy has an $R^{1/4}$ profile, then the flux beyond the SDSS Petrosian aperture accounts for an additional 0.22 mag, i.e.,

¹¹ Other authors have used $n = 2.5$ (e.g., Blanton et al. 2003b) or $R_{90}/R_{50} = 2.6$ (e.g., Strateva et al. 2001; Kauffman et al. 2003) to mark the rough divide between luminous early- and late-type galaxies.

roughly a fifth of that galaxy's total light. In this paper we outline a simple method for accurately recovering the missed flux.

Differences between galaxy light profile shapes result in a range of galaxy concentrations. We have shown how these can be used to correct for the flux outside of the Petrosian apertures and thus provide a galaxy's total (Sérsic) magnitude. The corrections presented here hold to the extent that Sérsic's $R^{1/n}$ model provides a good description of the various galaxy light profiles. For early-type galaxies this is known to be the case (e.g., Caon et al. 1993), while for late-type galaxies the correction is <0.06 mag and one can argue whether or not to apply it.

For typical elliptical galaxies, Petrosian magnitudes can fall shy of the total magnitude by a couple of tenths of a magnitude. Application of our method to the SDSS Petrosian magnitudes yielded total (Sérsic) magnitudes accurate to a couple of hundredths of a magnitude. Moreover, it actually provided a more accurate measurement of this quantity than is obtained from direct Sérsic fits to the data (Blanton et al. 2005).

We have shown how the galaxy concentration can also be used to determine the effective half-light radius R_e from the Petrosian radius R_p and thereby also leading to a determination of the associated surface brightness terms. We also provide magnitude corrections under the assumption that galaxy light profiles truncate at 5 effective radii.

In regard to the SDSS data, Blanton et al. (2005) showed how their Sérsic fits to objects with increasingly higher values of n resulted in increasingly underestimated effective radii. For example, their code obtained radii that were $\sim 80\%$ of the true effective radii for simulated objects with $n = 4.5$ ($R_{90}/R_{50} = 3.4$). Due to this, the concentration-corrected effective radii

derived from the Petrosian 50% radii are in fact preferable to those obtained from the direct Sérsic fits. The same is obviously true for the associated surface brightness terms. In passing, we warn that the use of $3R_p$, with $1/\eta(R_p) = 0.5$, misses more than half of an $R^{1/4}$ profile's flux and should therefore not be used in the analysis of bright elliptical galaxies. The use of $2R_p$, with $1/\eta(R_p) = 0.2$, as justified by the SDSS consortium, is suitably appropriate. The optimal choice of concentration remains an outstanding issue.

While the corrective scheme outlined here is general to any choice of Petrosian index and aperture, the tabulated values we have provided are specific to two commonly used Petrosian systems, namely, that used by CAS (Conselice 2003) and the setup adopted by the SDSS collaboration (York et al. 2000).

We are grateful for Michael Blanton's prompt and helpful replies to our assorted queries. We also wish to thank the anonymous referee for detailed comments.

C. J. C. acknowledges support from an NSF postdoctoral fellowship. M. A. B. acknowledges support from NSF grant AST-0307417. S. M. C. acknowledges support from STScI grant HST-AR-9917. S. P. D. acknowledges financial support from the Australian Research Council through DP0451426.

Funding for the Sloan Digital Sky Survey has been provided by the Alfred P. Sloan Foundation, the Participating Institutions, the National Aeronautics and Space Administration, the National Science Foundation, the US Department of Energy, the Japanese Monbukagakusho, and the Max Planck Society. The SDSS Web site is at <http://www.sdss.org/>.

REFERENCES

- Abazajian, K., et al. 2005, *ApJ*, 625, 613
 Bershad, M. A., Jangren, A., & Conselice, C. J. 2000, *AJ*, 119, 2645
 Bershad, M. A., Lowenthal, J. D., & Koo, D. C. 1998, *ApJ*, 505, 50
 Bland-Hawthorn, J., Vlahić, M., Freeman, K. C., & Drain, B. T. 2005, *ApJ*, 629, 239
 Blanton, M., et al. 2001, *AJ*, 121, 2358
 ———. 2003a, *ApJ*, 592, 819
 ———. 2003b, *ApJ*, 594, 186
 ———. 2005, *AJ*, 129, 2562
 Caon, N., Capaccioli, M., & D'Onofrio, M. 1993, *MNRAS*, 265, 1013
 Chang, R., et al. 2005, *MNRAS*, submitted (astro-ph/0502117)
 Ciotti, L. 1991, *A&A*, 249, 99
 Conselice, C. J. 2003, *ApJS*, 147, 1
 Conselice, C. J., Gallagher, J. S., III, & Wyse, R. F. G. 2002, *AJ*, 123, 2246
 Conselice, C. J., et al. 2003, *AJ*, 125, 66
 Cross, N. J. G., Driver, S. P., Liske, J., Lemon, D. J., Peacock, J. A., Cole, S., Norberg, P., & Sutherland, W. J. 2004, *MNRAS*, 349, 576
 Cross, N. J. G., et al. 2001, *MNRAS*, 324, 825
 Dalcanton, J. J. 1998, *ApJ*, 495, 251
 De Rijcke, S., Michielsen, D., Dejonghe, H., Zeilinger, W. W., & Hau, G. K. T. 2005, *A&A*, 438, 491
 de Souza, R. E., Gadotti, D. A., & dos Anjos, S. 2004, *ApJS*, 153, 411
 Djorgovski, S., & Davis, M. 1987, *ApJ*, 313, 59
 Djorgovski, S., & Spinrad, H. 1981, *ApJ*, 251, 417
 Dressler, A., et al. 1987, *ApJ*, 313, 42
 Driver, S. P., Liske, J., Cross, N. J. G., De Propriis, R., & Allen, P. D. 2005, *MNRAS*, 360, 81
 Dutton, A. A., van den Bosch, F. C., Courteau, S., & Dekel, A. 2005, preprint (astro-ph/0501256)
 Erwin, P., Beckman, J. E., & Pohlen, M. 2005, *ApJ*, 626, L81
 Faber, S. M., & Jackson, R. E. 1976, *ApJ*, 204, 668
 Goto, T., et al. 2003, *PASJ*, 55, 739
 Graham, A. W., & Driver, S. 2005, *Publ. Astron. Soc. Australia*, 22, 118
 Graham, A. W., Erwin, P., Caon, N., & Trujillo, I. 2001a, *ApJ*, 563, L11
 Graham, A. W., & Guzmán, R. 2003, *AJ*, 125, 2936
 Graham, A. W., Trujillo, I., & Caon, N., 2001b, *AJ*, 122, 1707
 Gunn, J. E., & Oke, J. B. 1975, *ApJ*, 195, 255
 Kauffmann, G., et al. 2003, *MNRAS*, 341, 54
 Kormendy, J. 1977, *ApJ*, 218, 333
 Lubin, L. M., & Sandage, A. 2001, *AJ*, 122, 1084
 Matković, A., & Guzmán, R. 2005, *ApJ*, submitted
 McIntosh, D. I., et al. 2005, *ApJ*, 632, in press (astro-ph/0411772)
 McLure, R. J., & Dunlop, J. S. 2004, *MNRAS*, 352, 1390
 Narayan, C. A., & Jog, C. J. 2003, *A&A*, 407, L59
 Norberg, P., et al. 2002, *MNRAS*, 336, 907
 Peng, C. Y., Ho, L. C., Impey, C. D., & Hans-Walter, W. 2002, *AJ*, 124, 266
 Petrosian, V. 1976, *ApJ*, 209, L1
 Pohlen, M., Beckman, J. E., Hüttemeister, S., Knapen, J. H., Erwin, P., & Dettmar, R.-J. 2004, *Ap&SS*, 319, 713
 Sandage, A., & Perlmutter, J.-M. 1990, *ApJ*, 350, 481
 Scodreggio, M. 2001, *AJ*, 121, 2413
 Sérsic, J. L. 1963, *Bol. Asoc. Argent. Astron.*, 6, 41
 ———. 1968, *Atlas de Galaxias Australes* (Cordoba: Obs. Astron.)
 Shankar, F., Salucci, P., Granato, G. L., De Zotti, G., & Danese, L. 2004, *MNRAS*, 354, 1020
 Shen, S., et al. 2003, *MNRAS*, 343, 978
 Shimasaku, K., et al. 2001, *AJ*, 122, 1238
 Simard, L., et al. 2002, *ApJS*, 142, 1
 Strateva, I., et al. 2001, *AJ*, 122, 1861
 Strauss, M. A., et al. 2002, *AJ*, 124, 1810
 Takamiya, M. 1999, *ApJS*, 122, 109
 Trujillo, I., Aguerri, J. A. L., Cepa, J., & Gutiérrez, C. M. 2001a, *MNRAS*, 321, 269
 ———. 2001b, *MNRAS*, 328, 977
 Trujillo, I., Graham, A. W., & Caon, N. 2001c, *MNRAS*, 326, 869
 Tully, R. B., & Fisher, J. R. 1977, *A&A*, 54, 661
 van der Kruit, P. C. 2001, in *ASP Conf. Ser. 230, Galaxy Disks and Disk Galaxies*, ed. G. José, S. J. Funes, & E. M. Corsini (San Francisco: ASP), 119
 Volonteri, M., Saracco, P., & Chincarini, G. 2000, *A&AS*, 145, 111
 Wirth, G. D., Koo, D. C., & Kron, R. G. 1994, *ApJ*, 435, L105
 Yagi, M., Kashikawa, N., Sekiguchi, M., Doi, M., Yasuda, N., Shimasaku, K., & Okamura, S. 2002, *AJ*, 123, 66
 Yasuda, N., et al. 2001, *AJ*, 122, 1104
 York, D. G., et al. 2000, *AJ*, 120, 1579